National Advisory Committee
for Aeronautics
MAILED
AUG 28 1939
To Library, L. M. A. L.

TECHNICAL NOTES

NATIONAL ADVISORY COMMITTEE FOR AERONAUTICS

No. 725

TANK TESTS TO DETERMINE THE EFFECTS OF THE CHINE FLARE OF A FLYING-BOAT HULL N.A.C.A. MODEL SERIES 62 AND 69

By Joe W. Bell and Roland E. Olson
Langley Memorial Aeronautical Laboratory

Washington
August 1939

NASA Technical Library
3 1176 01425 7167

NATIONAL ADVISORY COMMITTEE FOR AERONAUTICS

TECHNICAL NOTE NO. 725

TANK TESTS TO DETERMINE THE EFFECTS OF THE CHINE FLARE OF A FLYING-BOAT HULL N.A.C.A. MODEL SERIES 62 AND 69

By Joe W. Bell and Roland E. Olson

SUMMARY

Twenty-two models of flying-boat hulls were tested in the N.A.C.A. tank for the purpose of determining the effects on water resistance and spray of 13 variations in the transverse section of the bottom of the forebody and of three variations in the form of the afterbody. The forebodies were of the same over-all dimensions and differed in the type and amount of chine flare. The afterbodies included one with a pointed plan form and straight buttocks, one with a second step and straight buttocks, and one with a second step and concave buttocks. The depth of the step at the keel was the same in all models.

In general, the effect of chine flare on the resistance was small although, at speeds just above the hump, the resistance of forms with chine flare was generally less than the resistance of the form without chine flare. The chine flare reduced the height of the forward part of the spray where the spray leaves the chine of the model above the water level but had little effect on the spray where the chine of the model was below the water level. In cases of extreme flare, the spray forming just ahead of the step seemed to be higher.

It was concluded that model 62-AD, consisting of a forebody with a chine flare having a width of 0.083 beam and 5° angle, combined with an afterbody having a second transverse step and concave buttocks, was the best of the combinations tested. Charts for the determination of the resistance and the static properties of this model are given.

INTRODUCTION

Most seaplane hulls are built with transverse curvature in the sides of the V-bottom to reduce the height of the spray. In some hulls, the curvature extends from the keel to the chine and, in others, the curvature is in only the outer portions of the transverse sections. Curvature in only the outer portions is known as chine flare. The selection of the type of curvature for the transverse sections involves a compromise in which the designer must decide between a complex form of hull with controlled spray and a simple form with unsuppressed spray and, in general, must consider possible effects of the hydrodynamic forces on the hull. This selection of transverse sections has, in many cases, been made by intuition and has led to a wide variety of transverse sections.

Models having a large number of these varied sections have been tested in the N.A.C.A. tank but other variations in the forms of the models and in the nature of the tests have prevented direct comparisons of the effects of the transverse curvature. A series of five planing surfaces of different transverse sections was tested by Sottorf and the results are reported in reference 1. Valuable conclusions have been drawn from Sottorf's tests but the use of the data has been limited by the small number of models tested and by the fact that the models used were single planing surfaces and could not be tested throughout all the conditions at which a seaplane hull operates.

In the present investigation, the N.A.C.A. 62 series and 69 series of models were designed and tested at the N.A.C.A. tank to provide comparative data as to forces and spray for a systematic variation of chine flare with other variables of the form of the hull reduced to a minimum. Comparisons of the results of chine flare were made with models having three different types of afterbody.

The results of the tests show the effects of a wide range of variations of flare and provide a basis for selecting the chine flare for a seaplane hull of moderate loading (gross load coefficient, C_{Δ_0}, up to 0.7).

DESCRIPTION OF MODELS

The 62 and 69 series of N.A.C.A. tank models consist of 13 forebodies of varied transverse sections and three interchangeable afterbodies of different type. The lines of the parent model, 62-D, and the two additional afterbodies are shown in figures 1 and 2, respectively. The offsets of model 62-AD are given in table I.

The parent model of the series, N.A.C.A. model 62-D, consists of forebody 62, which is similar to the forebody of N.A.C.A. model 11-A (reference 2), and of an afterbody having a transverse second step and longitudinal curvature of the buttock lines (concave).

The transverse sections, at the maximum beam, of the forebodies used in the investigation are shown in figure 3. The sections of the type shown continue forward for about 50 percent of the length of the forebody and are varied from this point forward to fair into the bow. Each of the sections consists of a straight V of 22-1/2° dead rise at the center portion with a constant-radius flare at the outer portion and is identical with the corresponding section of the parent form except for the flared portion. The flare was varied in two ways: first, by changing the width of the curved portion and, second, by changing the angle of flare. The angle of flare is defined as the angle between the horizontal and the tangent to the flare drawn at the chine. Angles of flare below horizontal are considered positive.

The first method of varying the flare can be seen in the diagrams of the transverse sections of forebodies 62-A, 62-B, and 62-C or forebodies 69-A, 69-D, and 69-G (fig. 3). In these sections, the arcs of the flare were drawn in such a way as to be tangent to the 22-1/2° V-bottom at varied distances from the chine and to maintain a constant angle of flare. For sections having equal angles of flare, it can readily be seen that the section having the narrower width of flare will have the shorter radius of curvature.

The second method of varying the flare is shown in the sections of forebodies 62-A, 69-A, 69-B, and 69-C. In this method of variation, the width of the flare from the chine to the point of tangency with the straight portion was held at a constant ratio to the width of the section and the radii of curvature were selected in such a way as to have different angles of flare.

In all the variations of the transverse section, the height of the chine above the base plane was dependent upon the other variables and, consequently, the angle of dead rise measured from the keel to the chine varied widely with the changes in curvature. Since transverse sections of the afterbodies were not varied to match the sections of the forebodies, the depth of the steps measured at or near the chine varied with changes of chine flare and became very large in the cases of such forebodies as 69-H, 69-I, and 62-C, even though the depth of the step at the keel remained the same.

In addition to afterbody D, which was a part of the parent model, two afterbodies designated E and F (fig. 2) were used in the tests. Afterbody E differed from afterbody D in that the keel and the buttocks were straight from the main step to the second step and that the tail extension was slightly changed to match the section of the afterbody at the second step. One notable dependent variable was the angle between the keel of the afterbody and the keel of the tail extension. In afterbody D, the keel of the afterbody was tangent to the horizontal at the second step and the keel of the tail extension had an angle of 15° with the horizontal, forming an angle of 15° between the keels at the second step. In afterbody E, the afterbody keel and the tail-extension keel had angles of 8° and 14° 15', respectively, at the second step, forming an angle of only 6° 15' between keels. Afterbody F was identical with the afterbody of N.A.C.A. model 11-A, which is described in detail in reference 2.

The models were made of wood and painted with several coats of varnish. In order to insure a uniform surface on all models at the time of the tests, each model was varnished and rubbed to a smooth surface a few days before it was tested.

When forebodies and afterbodies were interchanged, the depth of the step measured at the keel was repeated to ± 0.02 inch, which is within the accuracy of the construction of wooden models. No measurable variation in the angle of afterbody keel resulted from separating and reassembling models.

The forebodies and the afterbodies of the series of models were tested in the following combinations:

Model	Forebody	Afterbody
62-D	62	D
62-AD	62-A	D
62-BD	62-B	D
62-CD	62-C	D
69-AD	69-A	D
69-BD	69-B	D
69-CD	69-C	D
69-DD	69-D	D
69-ED	69-E	D
69-FD	69-F	D
69-GD	69-G	D
69-HD	69-H	D
69-ID	69-I	D
62-E	62	E
69-AE	69-A	E
69-DE	69-D	E
69-GE	69-G	E
62-F	62	F
62-CF	62-C	F
69-AF	69-A	F
69-DF	69-D	F
69-GF	69-G	F

APPARATUS AND PROCEDURE

The tests were made in the N.A.C.A. tank, which is described in reference 3, using the towing gear described in reference 4. Several of the models were tested free to trim and all of the model combinations used were tested by the general method.

Free-to-Trim Tests

The free-to-trim tests were made using assumed values for the gross weight and the get-away speed of a hypothetical flying boat. The models were pivoted about a point corresponding to the assumed center of gravity of the complete flying boat and were balanced about this point. A lift corresponding to the lift of the wings of the flying boat was applied by means of the hydrofoil device described in reference 3. The lift applied by this device was measured by means of a spring dynamometer of small deflection.

In order to determine a suitable position for the center of gravity, model 62-D was tested at five center-of-gravity positions and model 62-AD was tested at two positions. All the positions investigated had the same vertical height (15.56 inches) above the keel at the step. The longitudinal locations of the center of gravity were as follows:

Position	Distance of c.g. forward of main step, in.
0	9.25
1	7.75
2	6.25
3	4.75
4	3.25

On the basis of the results of these tests, position 2, 6.25 inches forward of the step, was selected for the center-of-gravity position for the rest of the free-to-trim tests and as the position of the center of moments for the general tests.

General Tests

The general tests were made with a range of loads and speeds sufficient to make the data applicable for any gross load coefficient up to 0.7 at rest and for any speed thought to be practicable for the models. The range of trims was sufficient to determine the resistance at best trim for all loads and speeds within the schedule but was not sufficient to include zero trimming moment for all cases. The data for zero trimming moment were not obtained because of the large number of models in the series and the limited amount of time available for the investigation. This omission was considered permissible because the primary purpose of the project was to obtain comparative data and the obtaining of design data on all the models was considered unimportant. The free-to-trim tests provided data for comparative purposes at zero trimming moment.

RESULTS AND DISCUSSION

Force Data

The results of the tests were reduced to the usual coefficients based on Froude's law to make them independent of size. In this case, the beam at the main step was chosen as the characteristic dimension. The nondimensional coefficients are defined as follows:

Load coefficient, $C_\Delta = \Delta/wb^3$

Resistance coefficient, $C_R = R/wb^3$

Speed coefficient, $C_V = V/\sqrt{gb}$

Trimming-moment coefficient, $C_M = M/wb^4$

Draft coefficient, $C_d = d/b$

where

Δ is load on water, pounds.

w, specific weight of water, pounds per cubic foot. (63.3 for those tests, usually taken as 64 for sea water.)

b, beam at main step, feet.

R, resistance, pounds.

V, speed, feet per second.

g, acceleration of gravity, 32.2 feet per second per second.

M, trimming moment, pound-feet.

d, draft at main step, feet.

Any consistent system of units may be used. The moment data are referred to a point 6.25 inches forward of the step and 1.56 inches above the base line. Tail-heavy moments are considered positive. Trim is the angle between the base line of the model and the horizontal.

Selection of longitudinal position of center of gravity by free-to-trim tests.- The results of tests of model 62-D with the five different centers of gravity are shown in figure 4. In general, the effect of forward movements of the center of gravity was to reduce the trim at all speeds. This change of trim caused an increase in the resistance up to a speed coefficient, C_V, of about 2.0 and caused a reduction in the resistance at speed coefficients from 2.0 to 5.0. Forward movements of the center of gravity also increased the tendency to porpoise. At position 1, it was necessary to connect the trim dashpot to prevent porpoising and, at position 0, the porpoising became so violent that the free-to-trim test could not be carried to speed coefficients above 3.8.

On the basis of these results, positions 1 and 2 were considered the best for model 62-D and were therefore the only positions investigated for model 62-AD. Figure 5 shows the results of the tests of model 62-AD at these centers of gravity. The effects of shifting the center of gravity were essentially the same as they were for model 62-D. The tendency to porpoise, however, was worse than for model 62-D. The tendency of model 62-AD to porpoise when tested at position 1 was considered sufficient reason for the selection of position 2. There was some tendency for the model to porpoise at center-of-gravity position 2 but this tendency did not seem to be any more pronounced than for most models that have been tested free to trim in the N.A.C.A. tank.

Most models show a tendency to porpoise when tested by the free-to-trim method. At the present time, this tendency cannot be considered as a definite basis for the prediction of the porpoising characteristics of a full-scale flying boat. Experience having shown that porpoising occurs when the center of gravity of a flying boat is located too far forward, it is considered advisable to locate the center of gravity far enough aft to avoid violent porpoising in the model test. For this reason, position 2 was used as the center of gravity for free-to-trim tests and as the center of moments for the general tests throughout the remainder of the investigation.

Comparison of the effects of chine flare at best trim.- Figure 6 shows a comparison of resistance coefficient at best trim plotted against speed coefficient for four models

with an angle of flare of 5° and different widths of flare.* Increases in the width of the flare can be seen to result in slight reductions of resistance at the hump and in greater reductions in the intermediate speed range above the hump. Because of the small order of difference in resistance at high speeds and the inconsistencies found in comparing these differences, no conclusions are drawn for speed coefficients above 5.0.

A comparison of resistance coefficient at best trim plotted against speed coefficient for four models of different angles of flare and the same width of flare is shown in figure 7. This comparison shows that increasing the angle of flare caused small reduction in resistance at the hump and greater reductions in the intermediate speed range. A second hump appears in the resistance curves of model 69-CD (angle of flare, 45°). This second hump consistently occurs in the best-trim resistance curves of the models having an angle of flare of 45°.

The variation of the hump resistance at best trim with the angle of flare is shown in figure 8. In some cases, the scatter of the test points is greater than the probable effect of variations of flare but this plot seems to show the trends of the effects, particularly at high load coefficients. At load coefficients of 0.6 and 0.5, there is a trend toward lower resistance with increasing angle of flare and, in general, the resistance is lower for greater widths of flare. These effects, however, are too small to be considered important.

Figure 9 shows the effect of chine flare on resistance at best trim for a speed coefficient of 3.0. The decrease in resistance at this speed is relatively unimportant in the take-off of a seaplane, but the comparison is included because the greatest effect of chine flare occurs in this speed range. The data presented in the figure definitely show trends toward lower resistance with increased angle of flare and with increased width of flare.

Increases in the width of flare and in the angle of flare both reduce the dead rise of the model measured from

---

*For purposes of comparison with models of different widths of flare, model 62-D is considered to have zero width of flare; and, for comparison with models of different angles of flare, it is considered to have -22-1/2° angle of flare.

the keel to the chine and both have similar effects on the resistance. It therefore follows that the dead rise measured to the chine may be an important variable in the effect of chine flare. Figure 10 shows resistance coefficients at best trim for a speed coefficient of 3.0 plotted against angle of dead rise to the chine for 13 models of the present series and for four V-bottom planing surfaces with no chine flare (reference 5). For this speed coefficient, the effect of the dead rise to the chine for the model compares closely with the effect of dead rise for the planing surfaces at load coefficients of 0.5 and 0.4. At the lighter loads, the effects are not in very good agreement but this result might be expected because of the presence of the afterbody on the model. In each of the model tests of the present series, the afterbody was clear of the water at a speed coefficient of 3.0 when heavily loaded but was in the water at the same speed when lightly loaded. Since the afterbody of the flying boat carries a portion of the load at the hump and is struck by large quantities of spray at high speeds, a close agreement with planing-surface data cannot be expected in these speed ranges.

Comparison of the effects of chine flare on free-to-trim results.- The results of free-to-trim tests of four models having different widths of flare are shown in figure 11. The effect of increasing the width of flare was to cause the maximum trim and the maximum resistance to occur at a lower speed and to increase the resistance at the hump. The increase in the resistance at the hump was relatively small in changing from no flare (model 62-D) to $0.083b_1$ width of flare (model 62-AD) but was larger in changing from $0.083b_1$ width to the wider flares, where b_1 is width of any transverse section of the forebody. The resistance and the trim at speeds above the hump were less for the models having greater width of flare.

Figure 12 shows the free-to-trim results for three models of different angles of flare and a width of flare of $0.083b_1$. Increasing the angle of flare caused the resistance and the trim humps to occur at a lower speed and reduced the trim and the resistance at speeds above the hump. The same tendency was found with other widths of flare.

Comparison of afterbodies.- The resistance coefficient at best trim is plotted against speed coefficient in figure 13 for three models using the same forebody and different afterbodies. The greatest effect shown in this

comparison is a higher resistance below the hump for model 62-F, which has the pointed afterbody. At the hump, the resistance of model 62-E is slightly higher than that of the other models but, in general, there are no important differences.

Afterbody E gave some trouble with "sticking" at the second step, which is not apparent at best trim but can be seen in figure 14. This sticking occurred only at high speeds where the spray from the main step struck the afterbody and did not break away from the model at the second step but followed along the bottom of the tail extension. This effect caused a suction that increased the resistance. When afterbody D ran at similar conditions, the water broke away from the second step. A study of the lines of afterbodies D and E in figures 1 and 2 will show that the trouble with afterbody E is not wholly due to the straight buttocks but is probably caused by the combination of the shallow depth of the second step and the small angle between the keels of the afterbody and the tail extension.

A comparison of the free-to-trim results of models 62-D, 62-E, and 62-F is shown in figure 15. The trim and the resistance of model 62-D were lower than the trim and the resistance of the other models at the hump and at low speeds. The differences in resistance above the hump were not great enough to be of any importance.

During the tests, models using the F afterbody had a tendency to yaw at speeds below the hump speed. None of the combinations using the D or the E afterbody had this tendency.

As a result of these comparisons, the D afterbody is considered the best, with the F afterbody second. All the comparisons of forebodies given in this report are for models using the D afterbody but other comparisons not included show that the same trends exist for the same forebodies combined with the E or F afterbody. Likewise, the effect of changes in the afterbody was similar when any other forebody was used in the comparison.

Design charts for model 62-AD.- The amount of data accumulated in these tests was so great that its very bulk makes it unwieldy. Inasmuch as the larger part of it is of no detailed interest to the designer, it has been summarized and the complete results of only one model are included. Because the force tests show model 62-AD to be as

good as any in the series and the spray characteristics, to be discussed later, show it to be the best of the series, the design charts of model 62-AD are given in this report. Charts for the determination of the resistance and the trimming moment of model 62-AD are given in figure 16. This type of chart is discussed in detail in reference 6. Figure 17 gives curves for determining the trim and the draft of model 62-AD at rest.

Spray Characteristics

The spray created by the forebody of a planing model can be understood better if it is considered in two distinct classifications: (1) spray originating where the chine of the model is above the surface of the water, illustrated in section A-A of figure 18; and (2) the spray originating where the chine is below the surface of the water, illustrated in section B-B of the same figure. The spray illustrated in section A-A leaves the model approximately at the angle of flare of the forebody and can therefore be directed by a properly designed flare. When the angle of flare is below the horizontal, the spray leaves the chine with a downward component in this region and is deflected upward upon striking the surface of the water. During the tests, the height of this spray after being deflected was never great enough to be considered objectionable. The spray of the second classification is the result of an intricate combination of velocities and pressures and apparently cannot be controlled by chine flare of the types investigated. Extreme chine flares caused this type of spray to go higher and it is doubtful that any flare really reduced the spray created at this part of the model.

Figure 19 shows photographs of seven models of the series taken during runs at about the hump speed with the load and the trim approximately equal to the load and the trim at which an application of one of these models would operate. These photographs show that the spray was lower in general for all the models with chine flare than for model 62-D, which had straight V sections and an angle of dead rise of 22-1/2°. In these photographs, the spray that leaves the model above the water line is more easily seen than the spray that originates where the chine is below the water line but the spray that originates where the chine is below the water line can be seen in some of the photographs by a study of the front views and the plan views together. Model 62-AD seems to cause less spray at this condition

than any of the other models but there is little difference between it and model 69-AD. Similar photographs of the same models taken at a load coefficient, C_{Δ}, of 0.62, about 20 percent greater load than that of the models in figure 19, showed the same effects of the chine flare.

Photographs showing the effect of chine flare on the spray at speeds above the hump are shown in figures 20 and 21. These photographs represent two different speeds with loads corresponding to the conditions of the free-to-trim tests and with a trim of 5°, which is near best trim for both speeds. Figure 20 shows that the effect of chine flare is about the same at intermediate speeds as at the hump. A comparison of the photographs in figure 21 shows that the spray is only slightly affected by the chine flare at a high speed and a light load just before get-away. At this speed and load, the entire chine of the forebody is above the water surface and a large portion of the spray comes from behind the step.

Such chine flares as those of models 62-CD, 69-HD, and 69-ID (fig. 3), not included in the photographs, caused higher spray where the chine was below the water line. The forward part of the spray where the chine was above the water line was little affected by excessive flare.

CONCLUSIONS

1. The height of the spray originating where the chine of the model was above the water level was reduced by the chine flare.

2. The height of the spray originating at the side of the portion of the chine that was below the water level was not reduced by the chine flare. In some cases, the height of this spray was increased by chine flare.

3. The resistance at best trim at the hump and at high speeds was only slightly affected by chine flare.

4. The resistance at best trim at intermediate planing speeds was reduced by chine flare.

5. In the free-to-trim tests, the trim and the resistance at the hump were increased by chine flare.

6. When all effects of the chine flare are considered, model 62-AD seems to be the best of the models tested in this investigation.

Langley Memorial Aeronautical Laboratory,
National Advisory Committee for Aeronautics,
Langley Field, Va., June 6, 1939.

REFERENCES

1. Sottorf, W.: Experiments with Planing Surfaces. T.M. No. 739, N.A.C.A., 1934.

2. Parkinson, John B.: A Complete Tank Test of a Model of a Flying-Boat Hull - N.A.C.A. Model No. 11-A. T.N. No. 470, N.A.C.A., 1933.

3. Truscott, Starr: The N.A.C.A. Tank - A High-Speed Towing Basin for Testing Models of Seaplane Floats. T.R. No. 470, N.A.C.A., 1933.

4. Allison, John M.: Tank Tests of a Model of the Hull of the Navy PB-1 Flying Boat - N.A.C.A. Model 52. T.N. No. 576, N.A.C.A., 1936.

5. Shoemaker, James M.: Tank Tests of Flat and V-Bottom Planing Surfaces. T.N. No. 509, N.A.C.A., 1934.

6. Dawson, John R.: A General Tank Test of a Model of the Hull of the P3M-1 Flying Boat Including a Special Working Chart for the Determination of Hull Performance. T.N. No. 681, N.A.C.A., 1938.

TABLE I

Offsets for N.A.C.A. Model 62-AD Flying-Boat Hull (Inches)

Station	Distance from F.P.	Distance from base line			Half-breadths		Radius of flare
		Keel	Chine	Tangency of flare	Chine	Tangency of flare	
F.P.	0	4.00	4.00		0.25		
1/2	2.40	9.33	5.12	5.52	2.25	1.88	0.94
1	4.80	11.00	6.19	6.55	3.81	3.18	.85
1½	7.20	12.01	7.14	7.48	5.03	4.19	1.05
2	9.60	12.67	7.93	8.25	5.96	4.97	1.29
3	14.40	13.34	9.12	9.38	7.22	6.02	1.70
4	19.20	13.50	9.91	10.15	7.94	6.62	2.39
5	24.00	13.58	10.32	10.54	8.29	6.91	2.80
6	28.80	13.66	10.52	10.75	8.45	7.04	3.13
7	33.60	13.75	10.60	10.82	8.50	7.08	3.02
8	38.40	13.83	10.68	10.90	↑	↑	↑
9	43.20	13.92	10.77	10.99	↓	↓	↓
10,F	48.00	14.00	10.85	11.07	8.50	7.08	3.02
10,A	48.00	13.44	9.92		8.50		
11	52.80	12.77	9.28		8.42		
12	57.60	12.09	8.70		8.19		
13	62.40	11.42	8.18		7.81		
14	67.20	10.74	7.74		7.24		
15	72.00	10.15	7.43		6.56		
15½	54.40	9.92	7.37		6.15		
16	76.80	9.77	7.40		5.73		
16¼,F	78.00	9.75	7.47		5.50		
16¼,A	78.00	9.50	7.22		5.50		
17	81.60	8.53	6.55		4.78		
18	86.40	7.25	5.69		3.76		
19	91.20	5.96	4.86		2.65		
20	96.00	4.68	4.06		1.49		
A.P.	100.80	3.39	3.27		.30		

Straight line

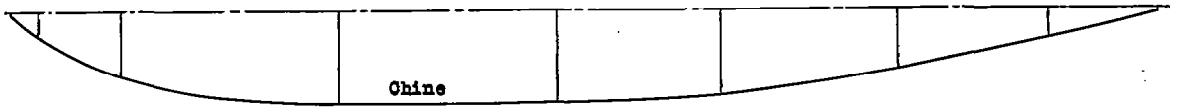

Half-breadth

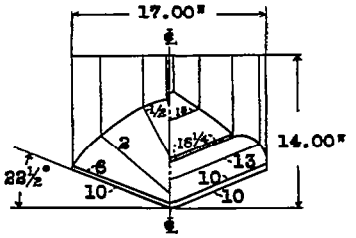

Body plan

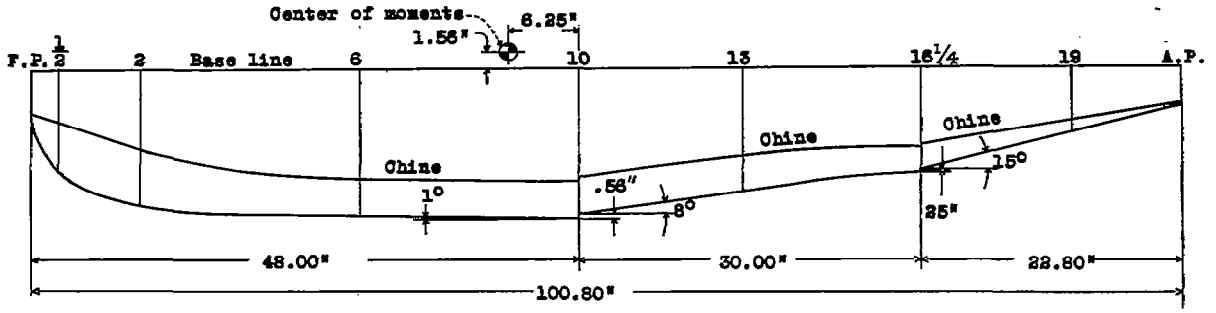

Profile

Figure 1.- Lines of N.A.C.A. model 62-D.

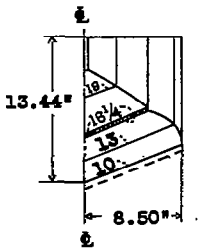

Body plan

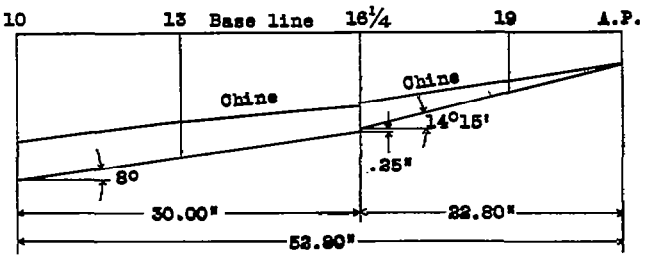

Profile

Afterbody E

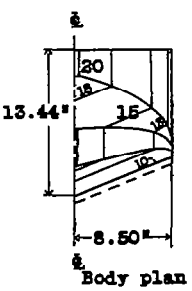

Body plan

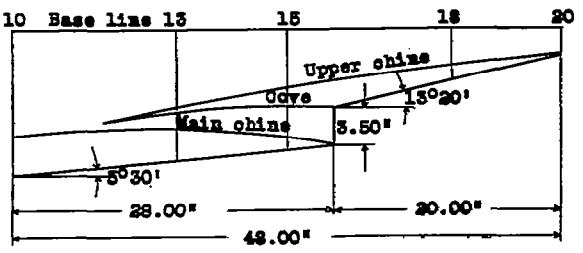

Profile

Afterbody F

Figure 2.- Lines of afterbodies E and F.

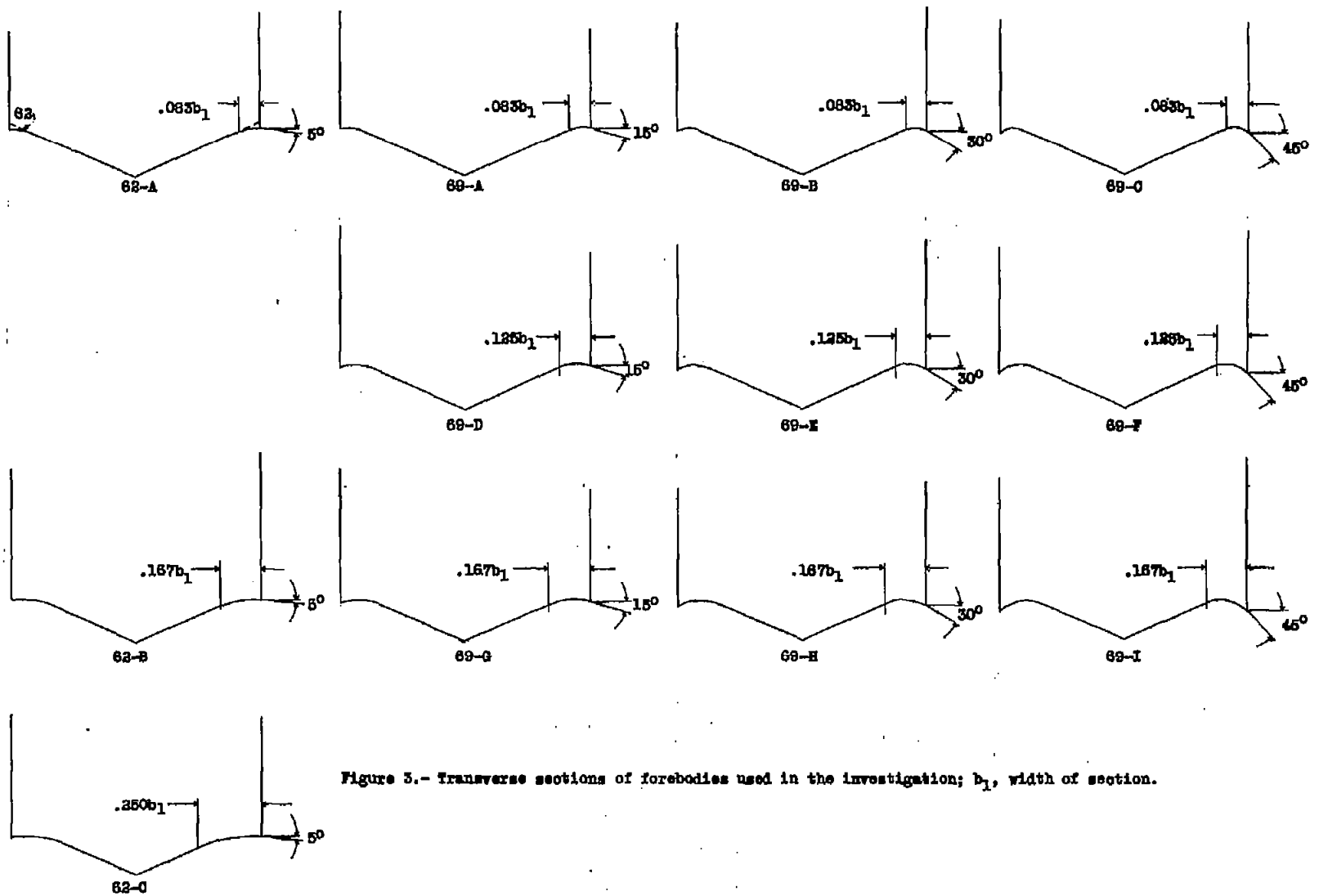

Figure 3.- Transverse sections of forebodies used in the investigation; b_1, width of section.

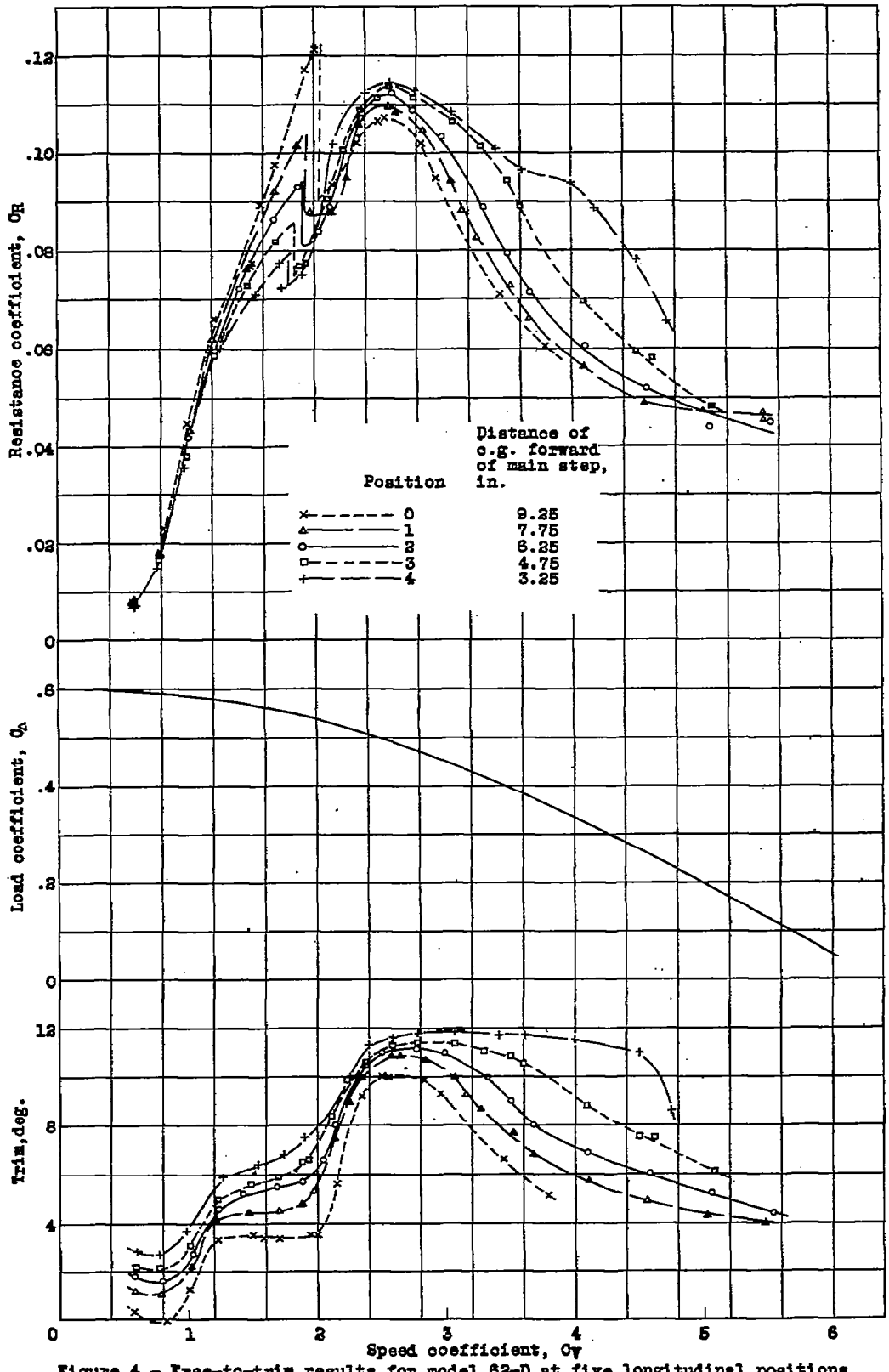

Figure 4.- Free-to-trim results for model 62-D at five longitudinal positions of the center of gravity.

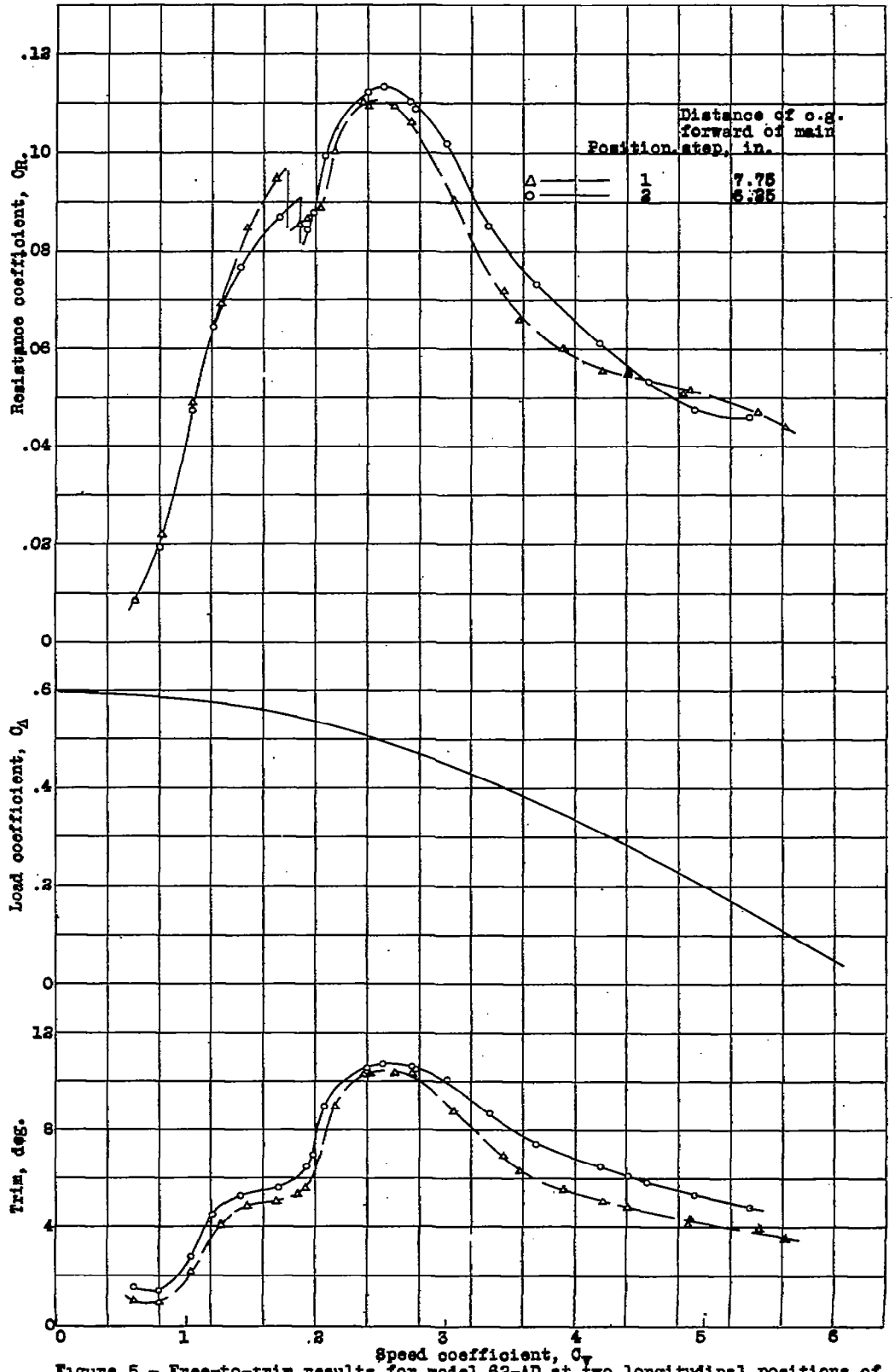

Figure 5.- Free-to-trim results for model 62-AD at two longitudinal positions of the center of gravity.

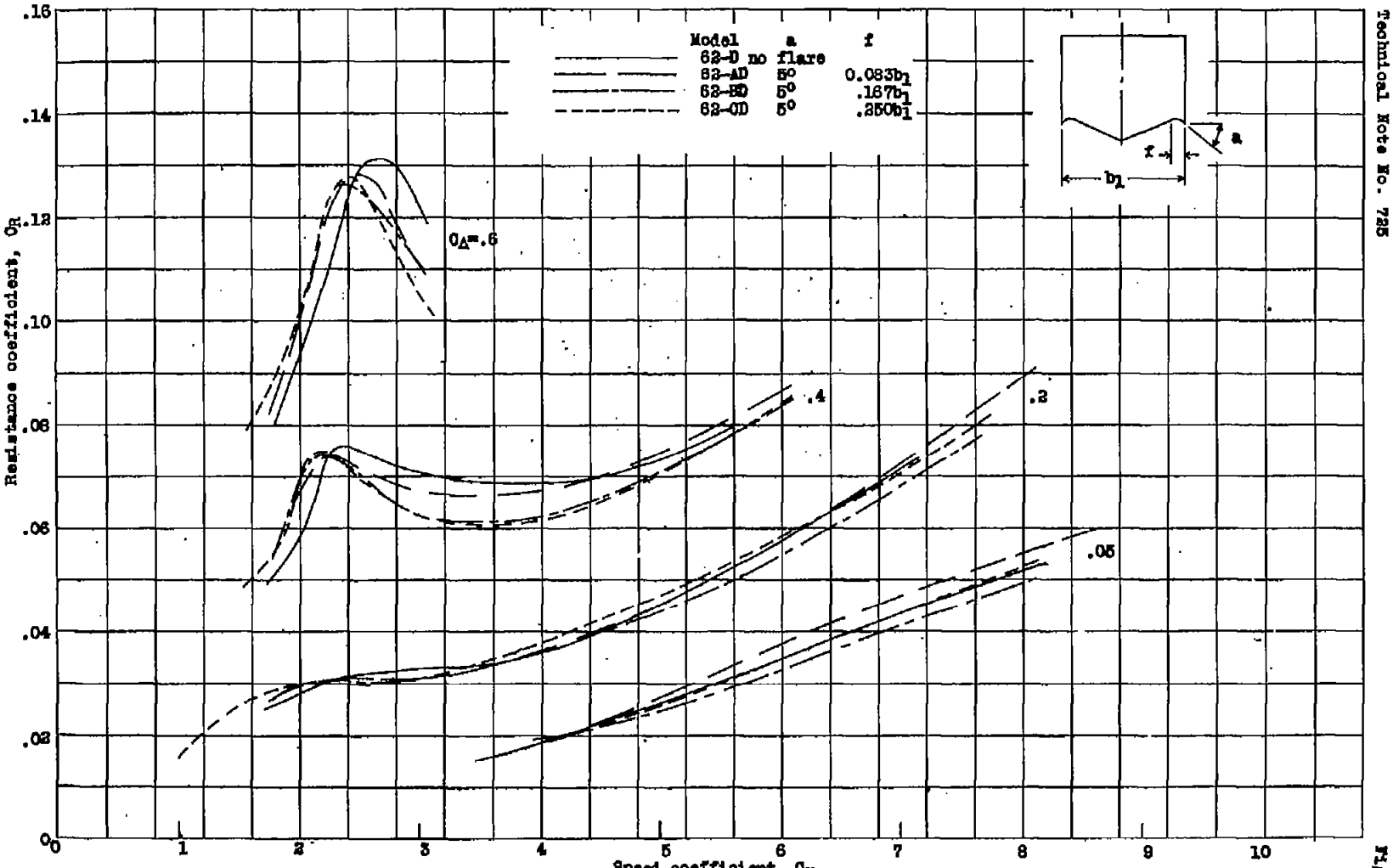

Figure 6.- Comparison of resistance coefficient at best trim for models having different widths of flare. Models 62-D, 62-AD, 62-BD, and 62-CD.

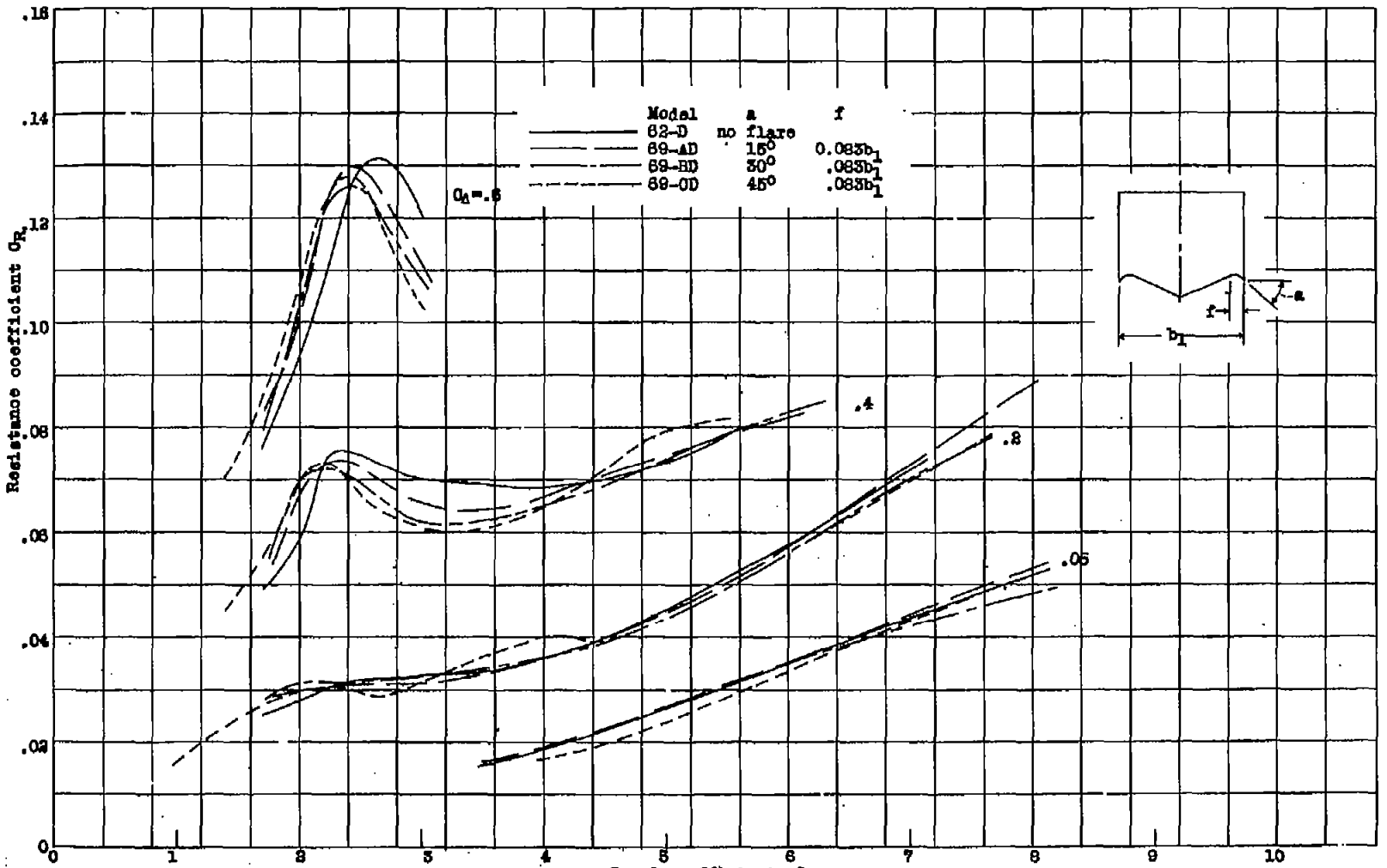

Figure 7.- Comparison of resistance coefficient at best trim for models having different angles of flare. Models 62-D, 69-AD, 69-BD, and 69-CD

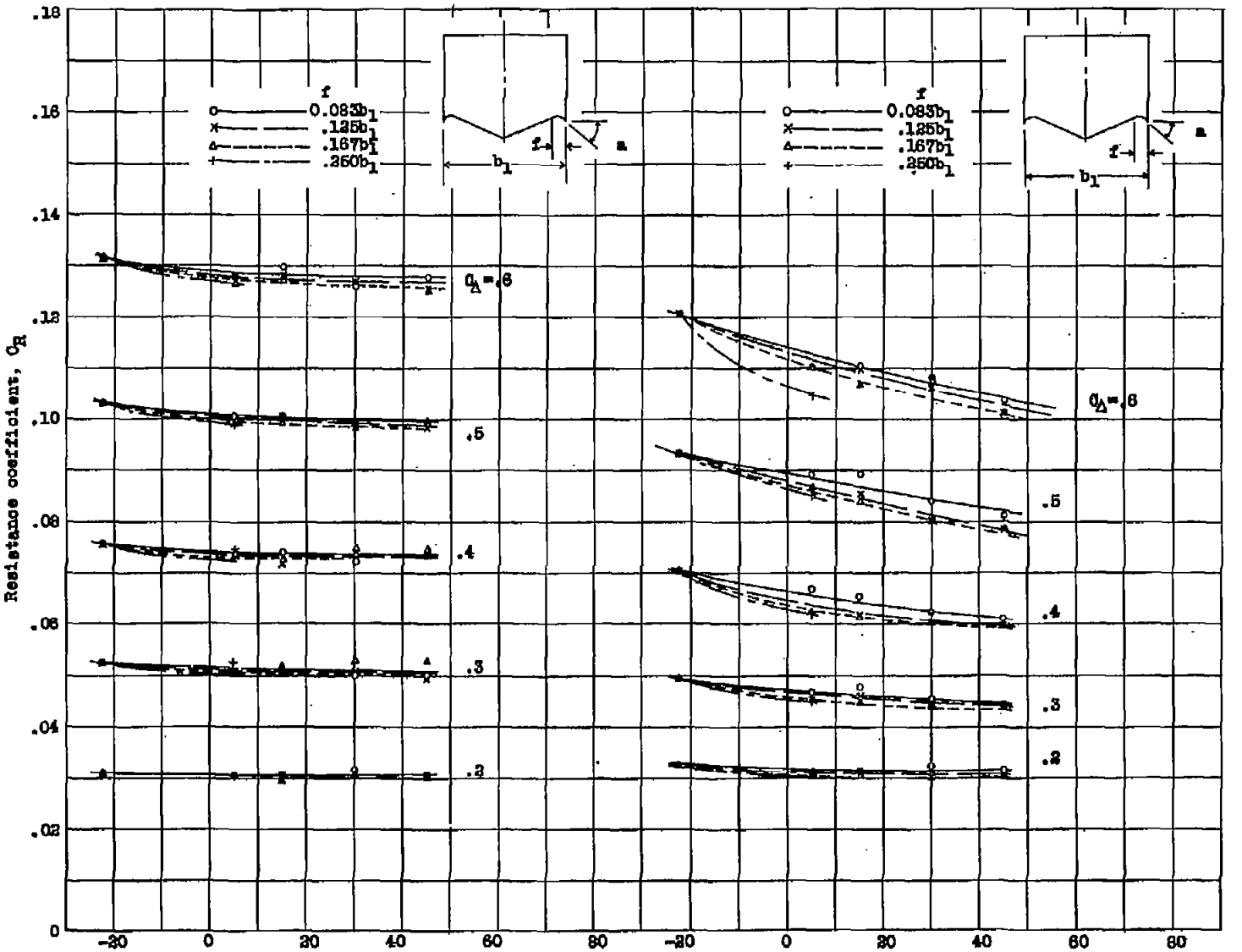

Figure 8.- Variation of hump resistance coefficient at best trim with angle of flare and width of flare.

Figure 9.- Variation of resistance coefficient, $C_\forall = 3.0$, at best trim with angle of flare and width of flare.

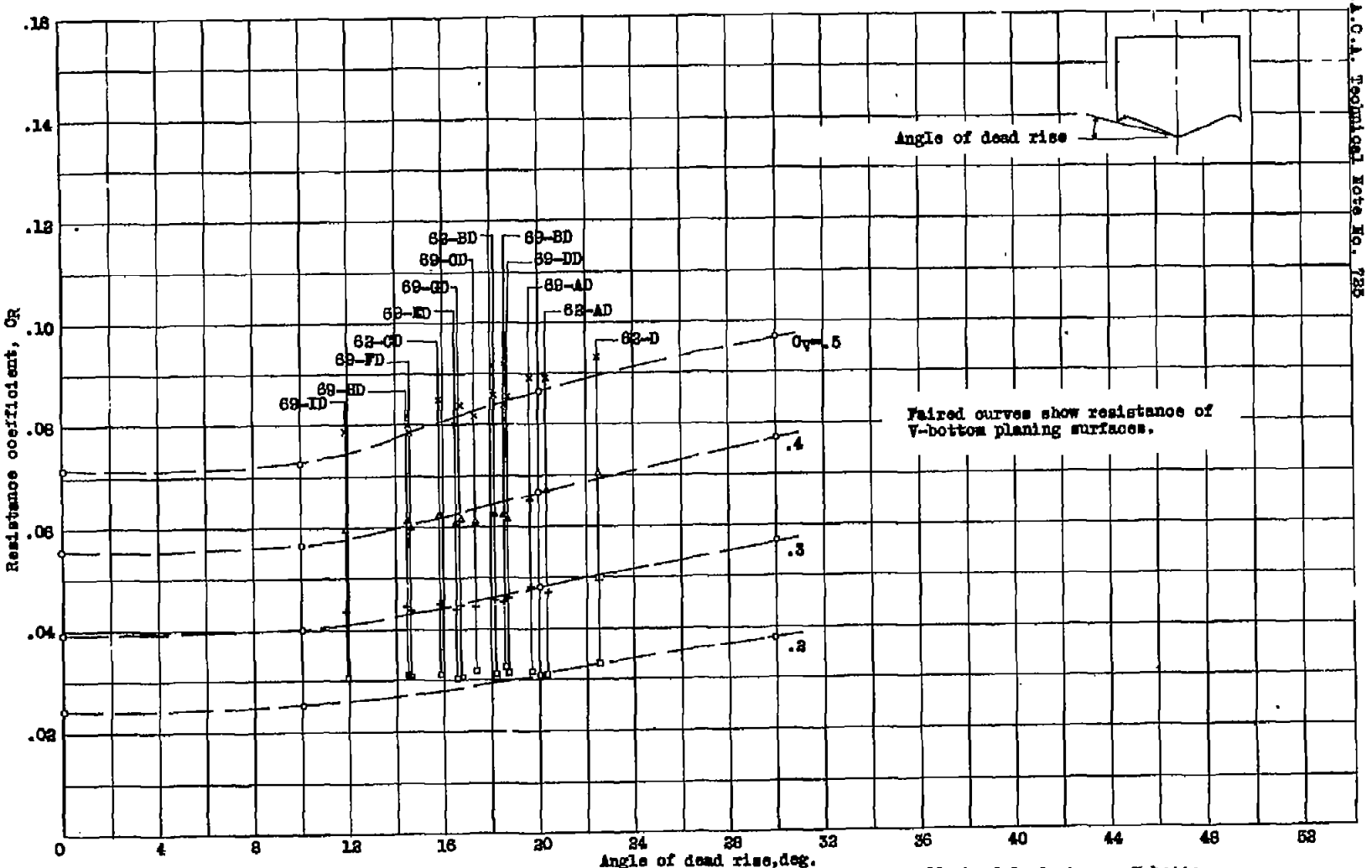

Figure 10.- Comparison of the effect of flare on a flying-boat model with the effect of dead rise on V-bottom planing surfaces. C_V=3.0.

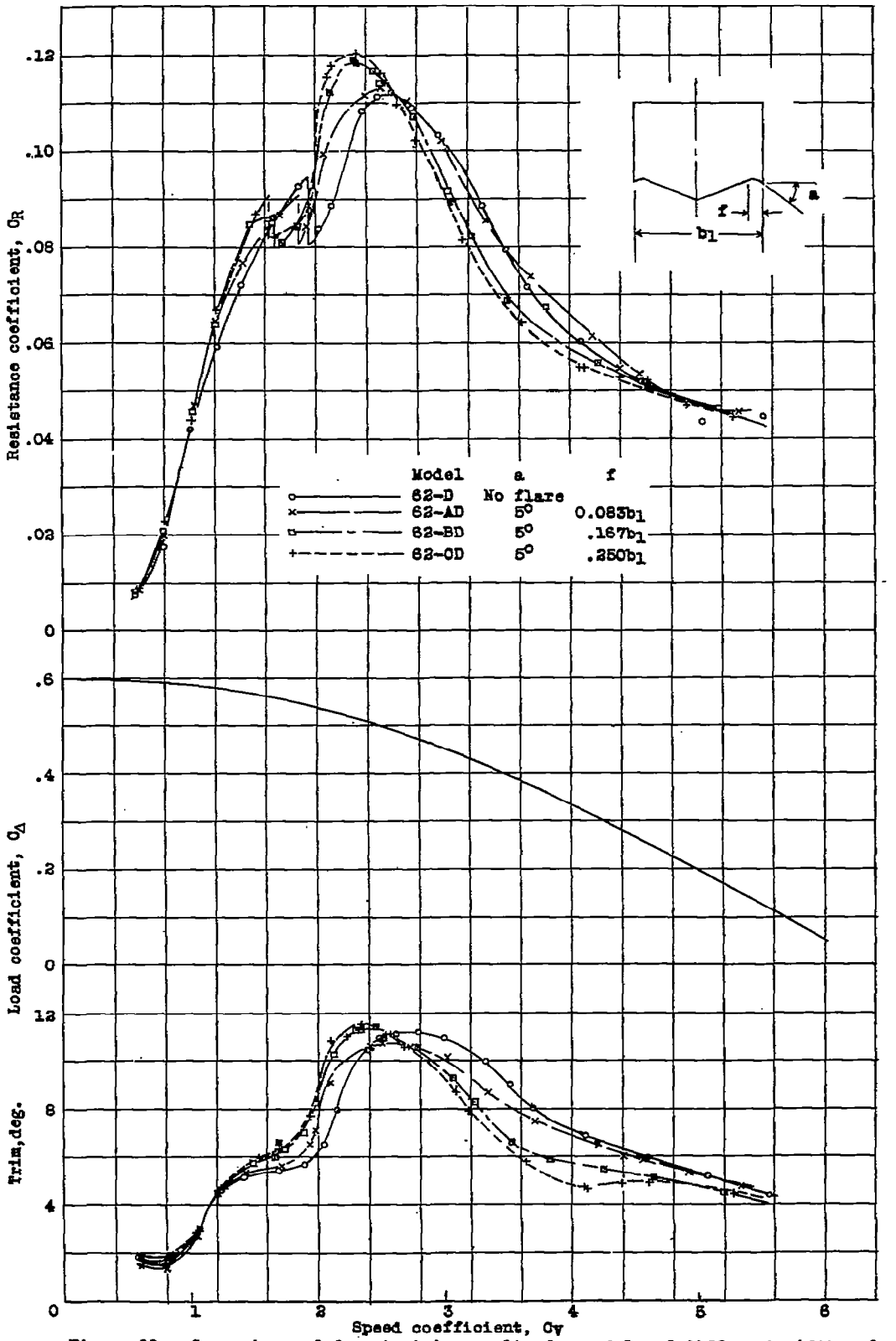

Figure 11.- Comparison of free-to-trim results for models of different widths of flare. Models 62-D, 62-AD, 62-BD, 62-CD.

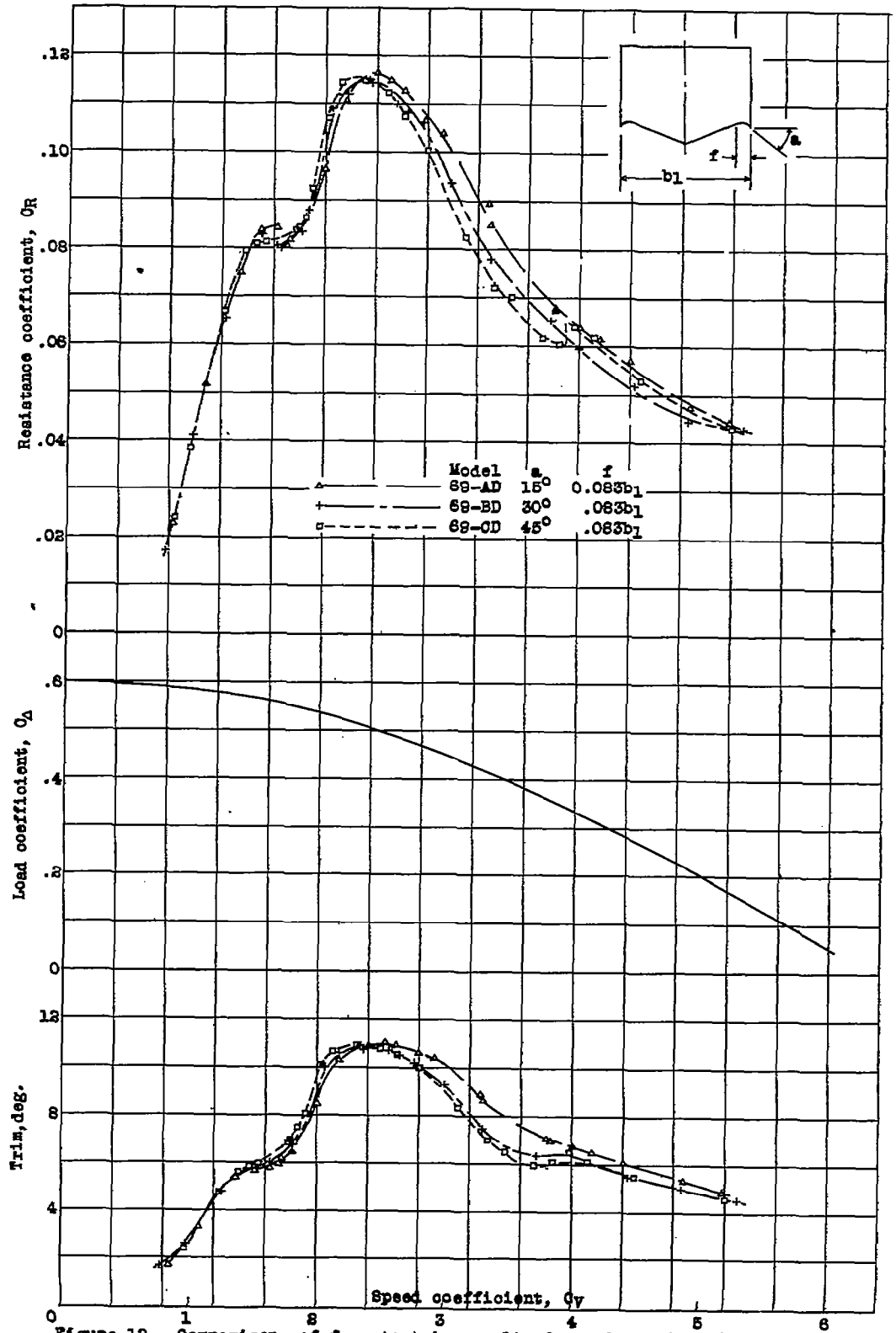

Figure 12.- Comparisons of free-to-trim results for models of different angles of flare. Flare-width, 0.083b_1. Models 69-AD, 69-BD and 69-CD.

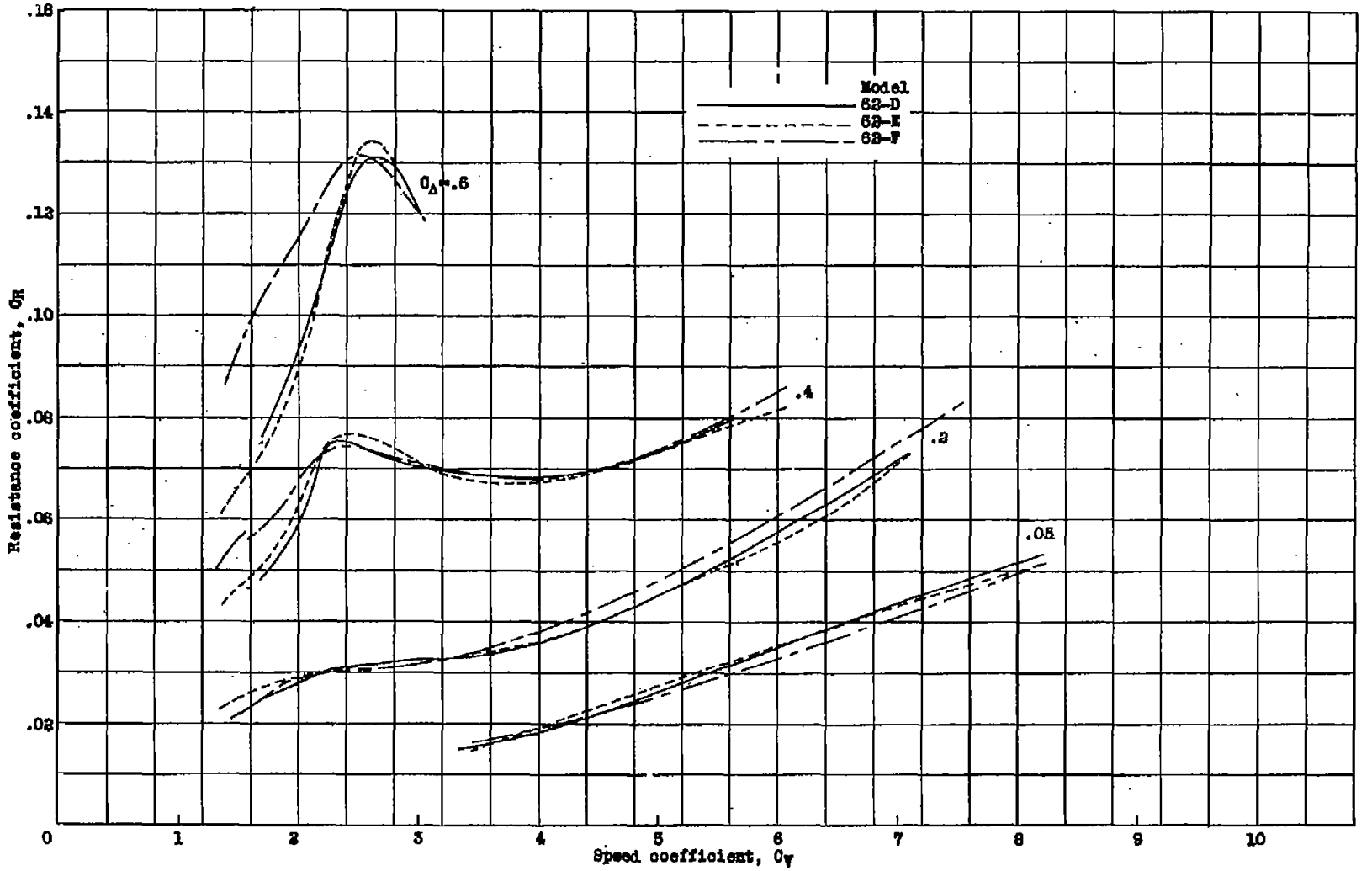

Figure 13.- Comparison of resistance coefficient at best trim for models having the same forebody and different afterbodies. Models 62-D, 62-E, and 62-F.

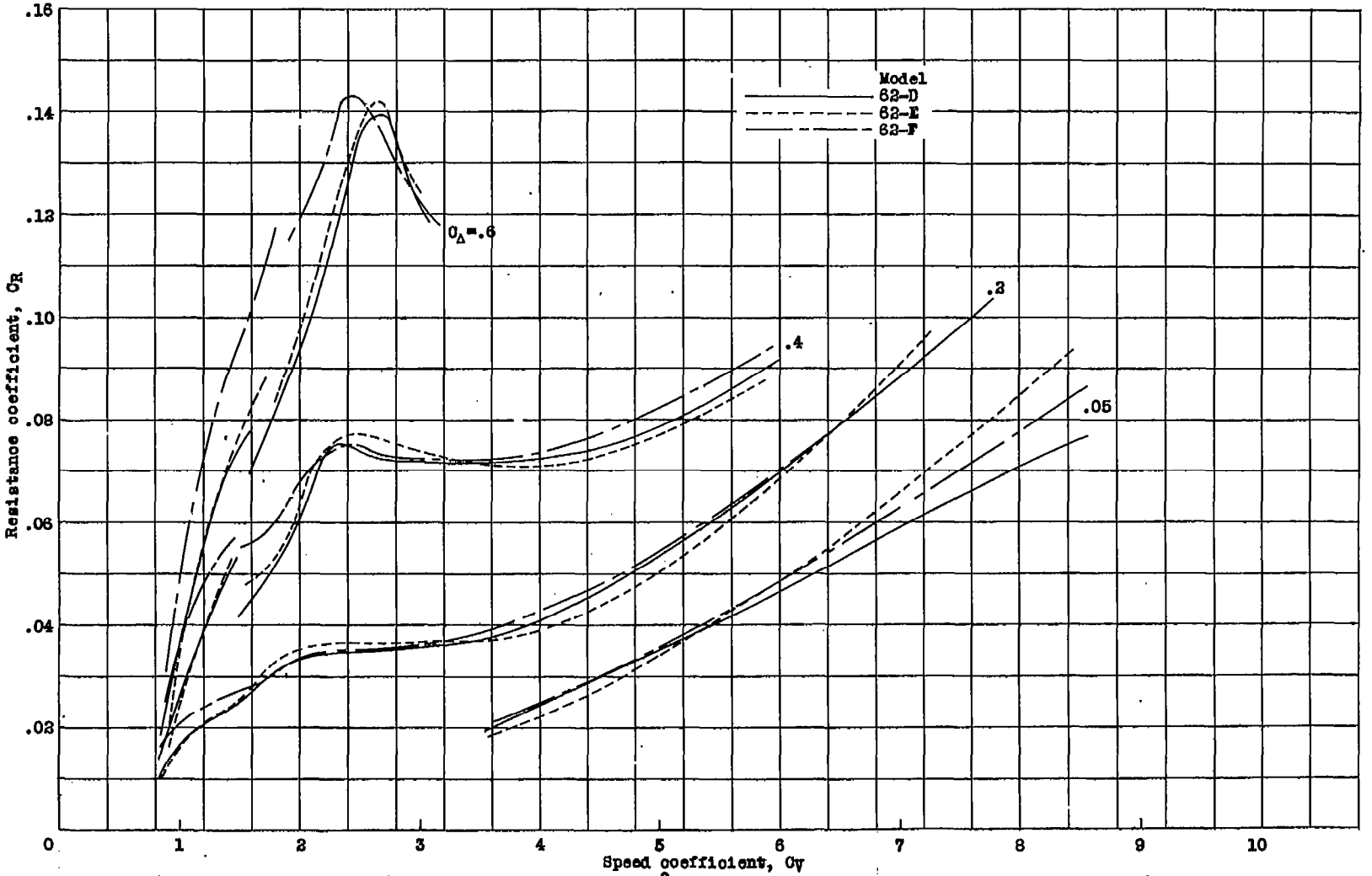

Figure 14.- Comparison of resistance coefficient at 7° trim for models having the same forebody and different afterbodies. Models 62-D, 62-E, and 62-F.

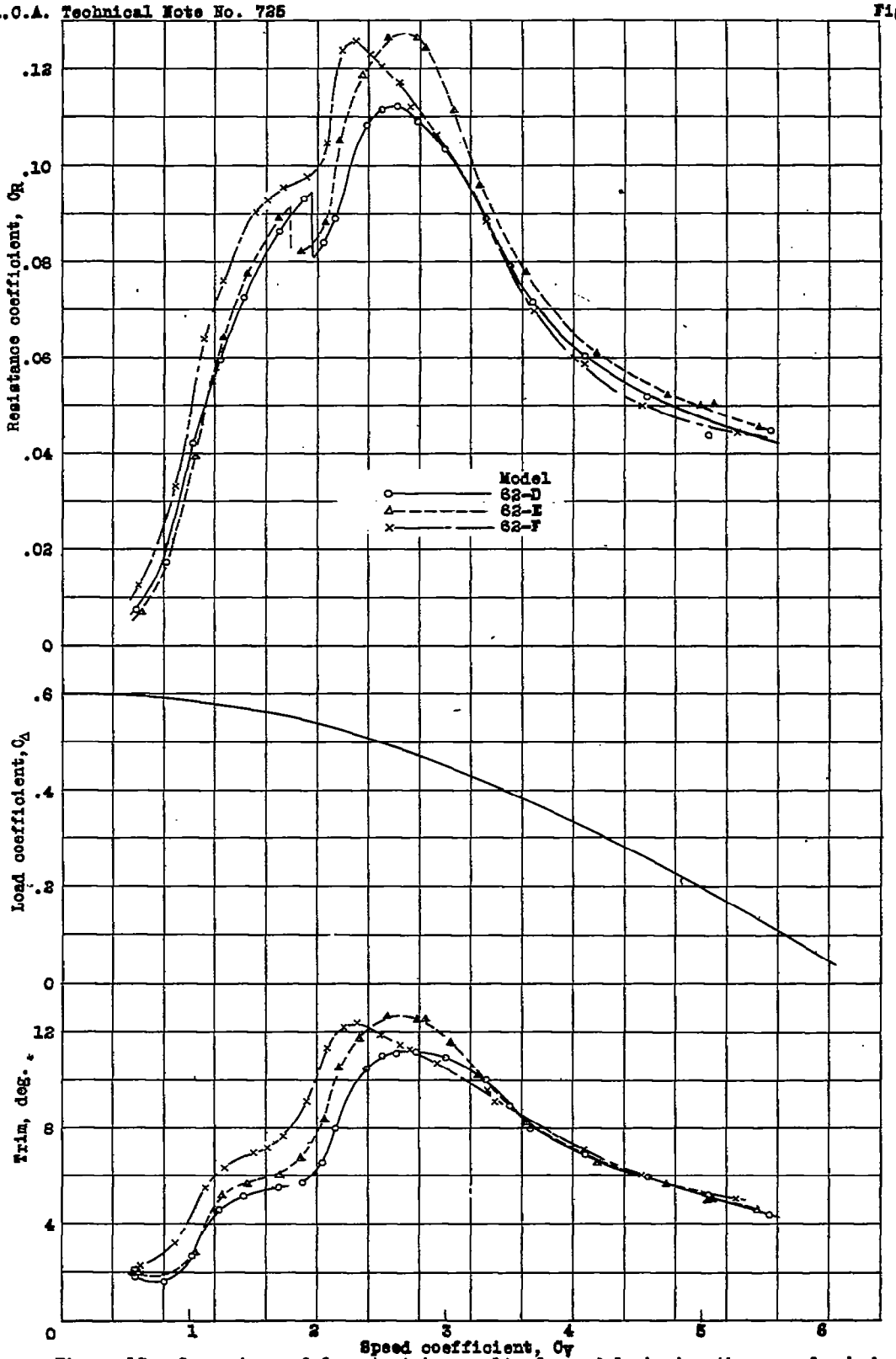

Figure 15.- Comparison of free-to-trim results for models having the same forebody and different afterbodies. Models 62-D, 62-E, and 62-F.

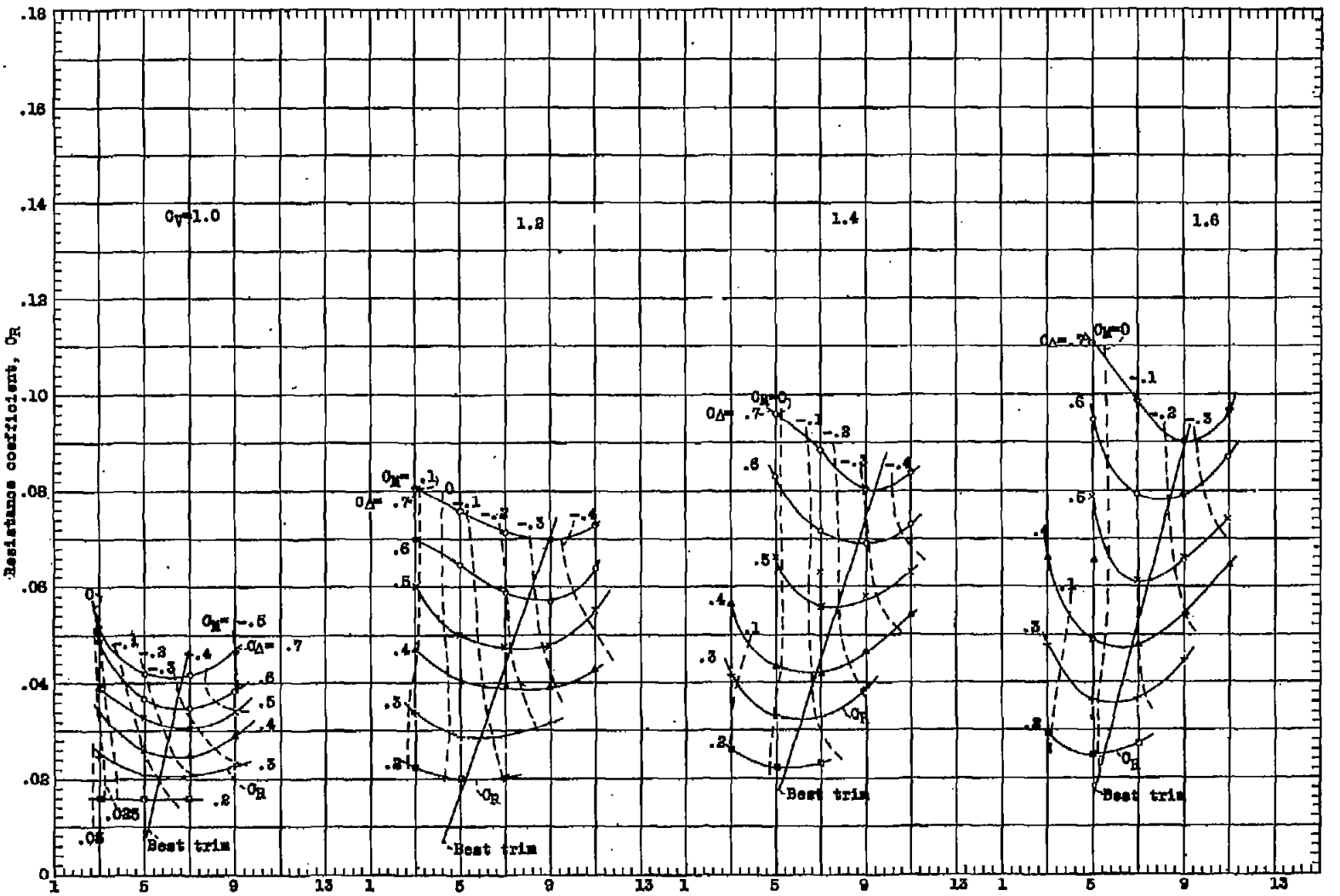

Figure 16a.- Model 62-AD. Working charts for the determination of resistance and trimming moment.

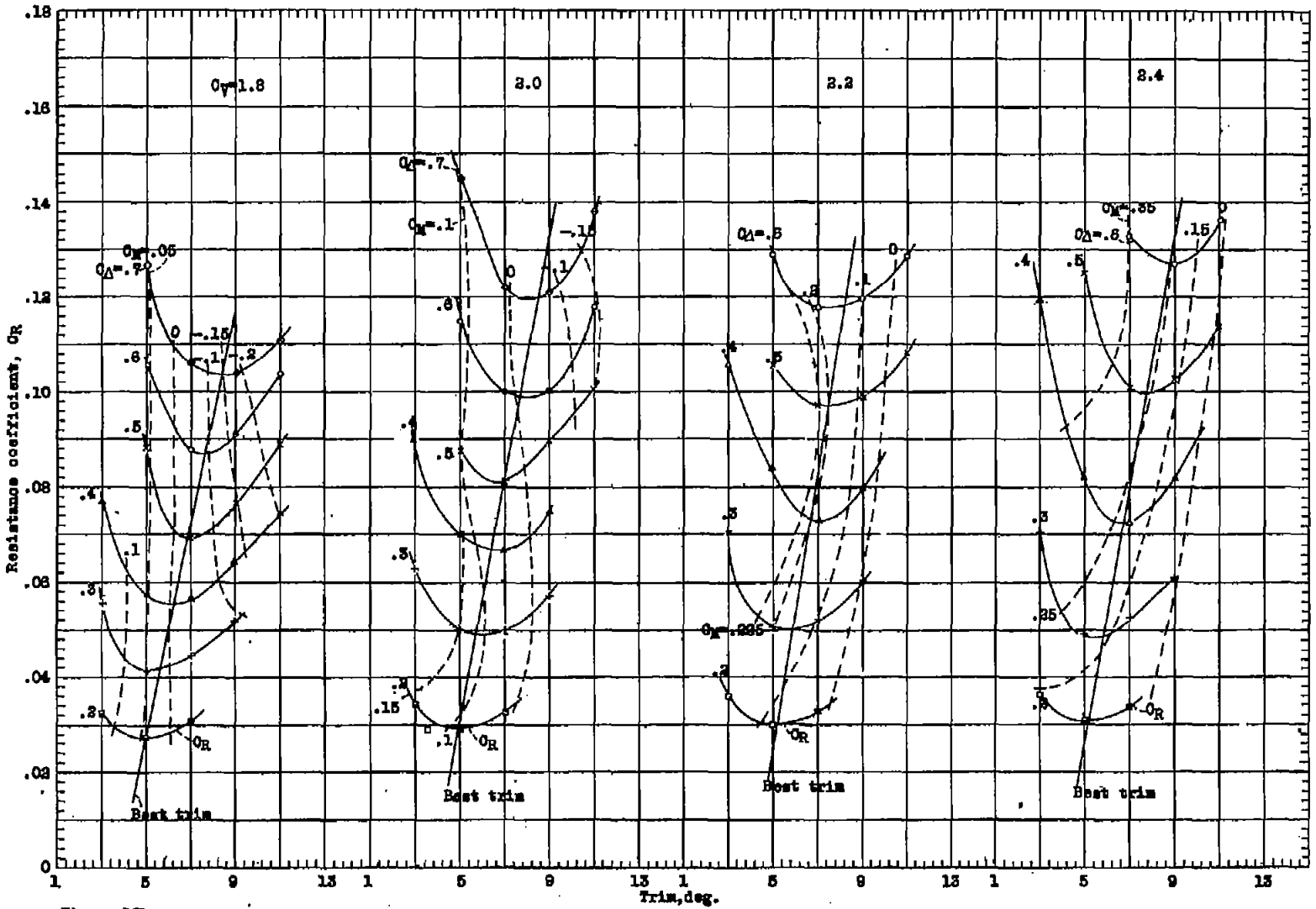
C_Y=1.8
2.0
2.2
2.4
Resistance coefficient, C_R
Trim, deg.
Best trim
C_R

Figure 16b.

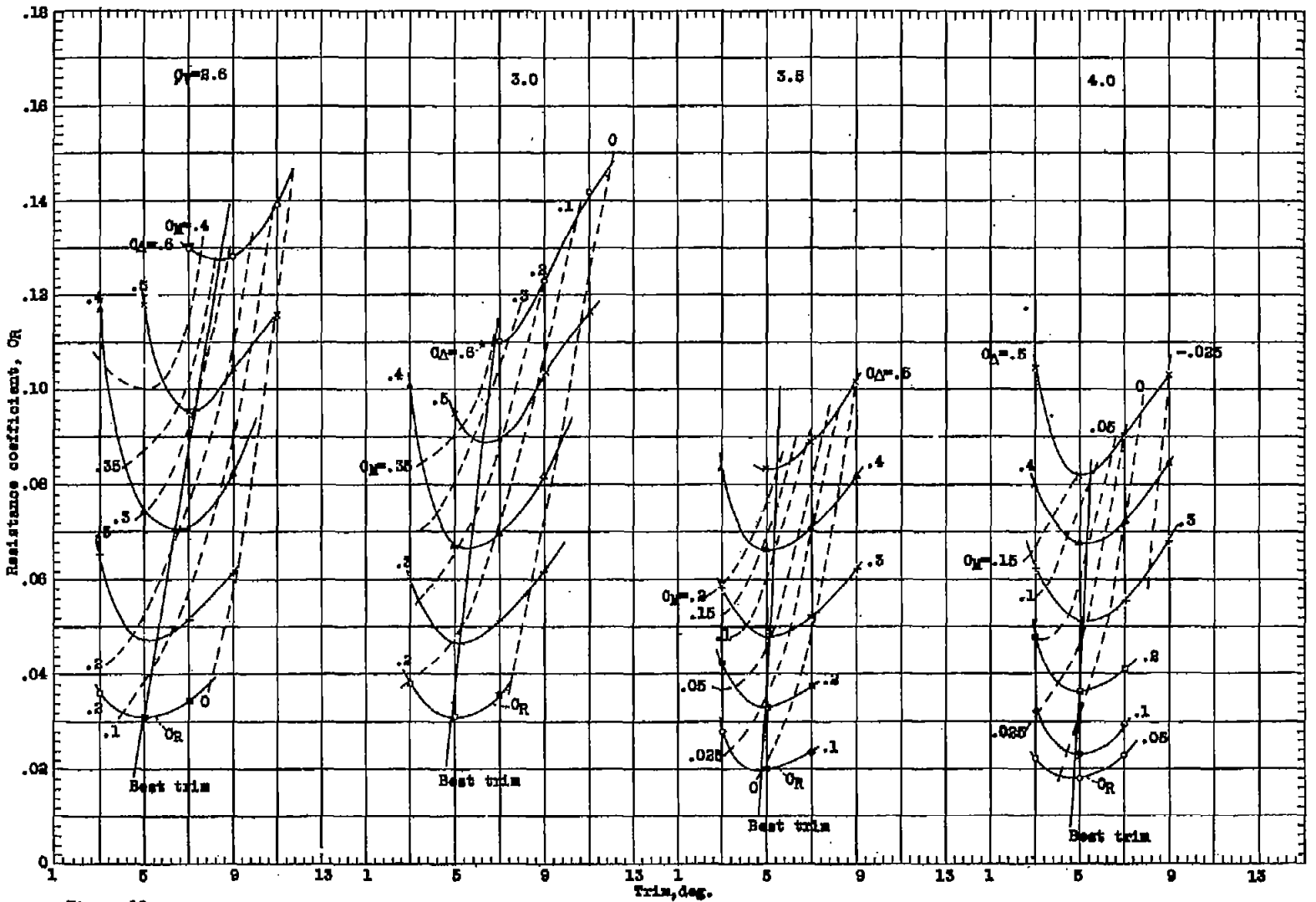
3.0
3.5
4.0
Resistance coefficient, C_R
Trim, deg.
Best trim
C_{L_Δ}=.6
C_{L_M}=.4
C_{L_M}=.35
C_{L_M}=.2
C_{L_M}=.15
C_{L_Δ}=.5
-.025
.05
.025
C_R

Figure 16c.

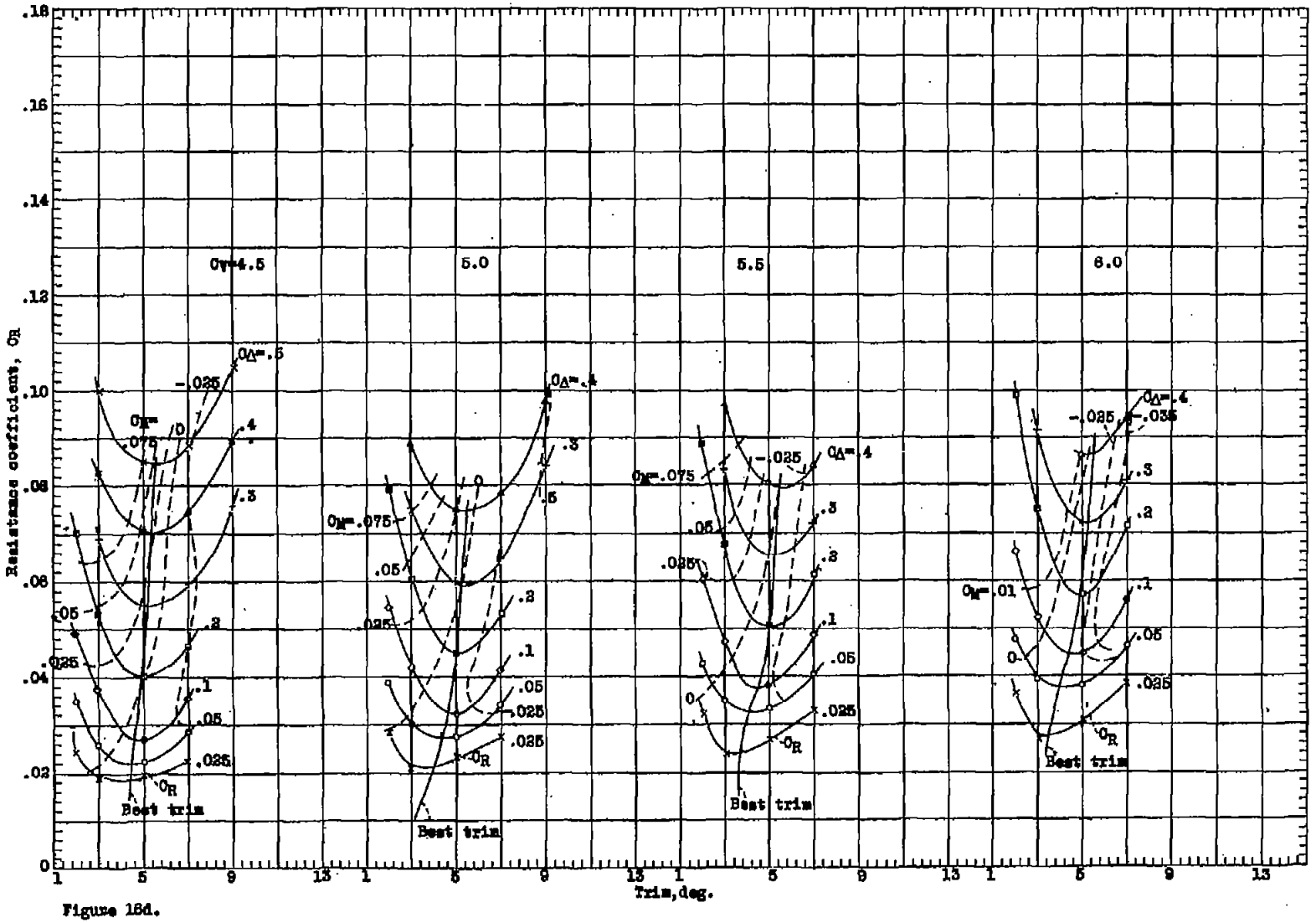
Cγ=4.5
5.0
5.5
6.0
Resistance coefficient, CR
Trim, deg.
Best trim
CR

Figure 16d.

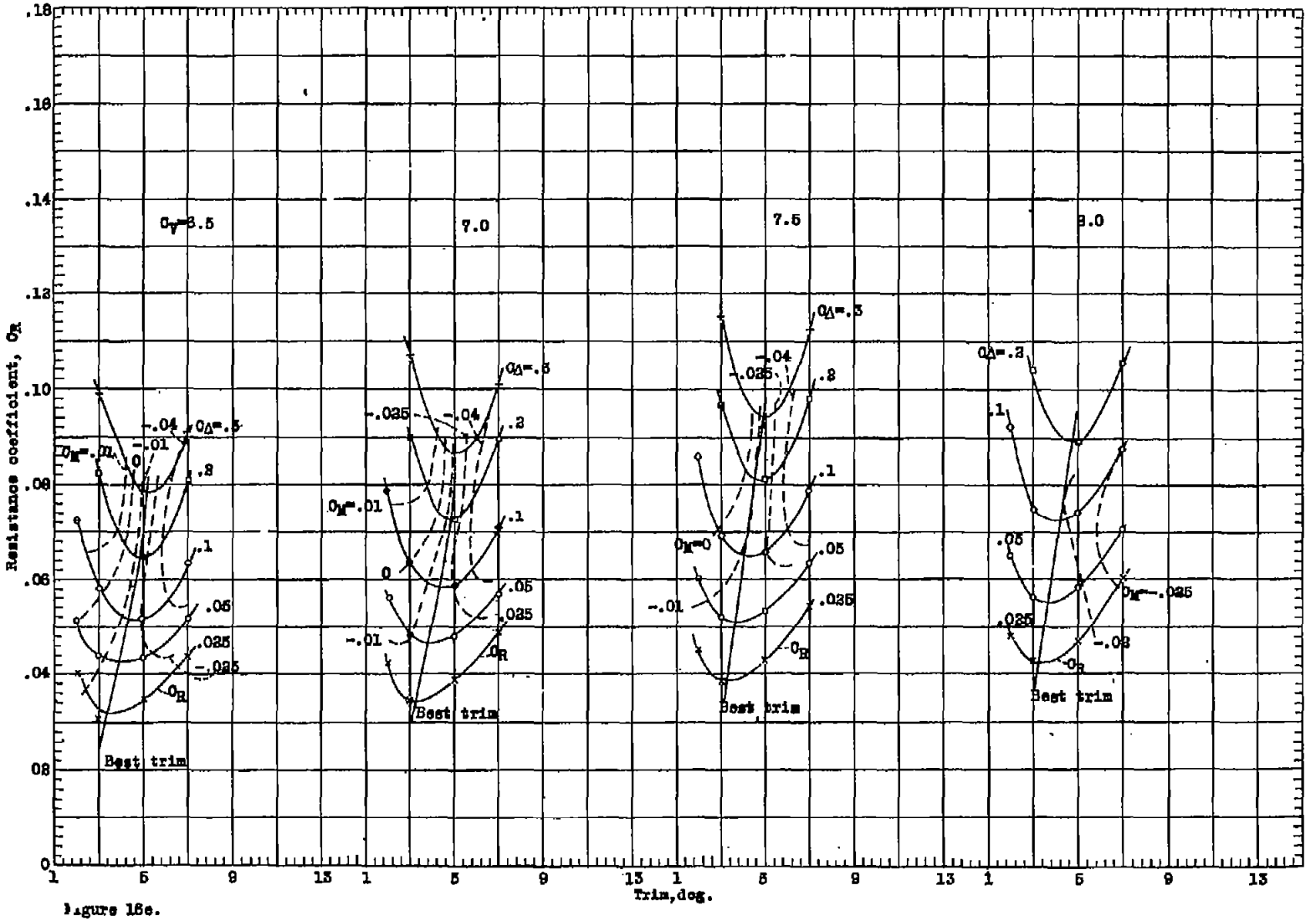
Resistance coefficient, C_R
Trim, deg.
C_Y=6.5
7.0
7.5
8.0
C_Δ=.3
.2
.1
.05
.025
0
-.01
-.025
-.04
C_M=.01
C_M=0
C_M=-.025
C_R
Best trim

Figure 16e.

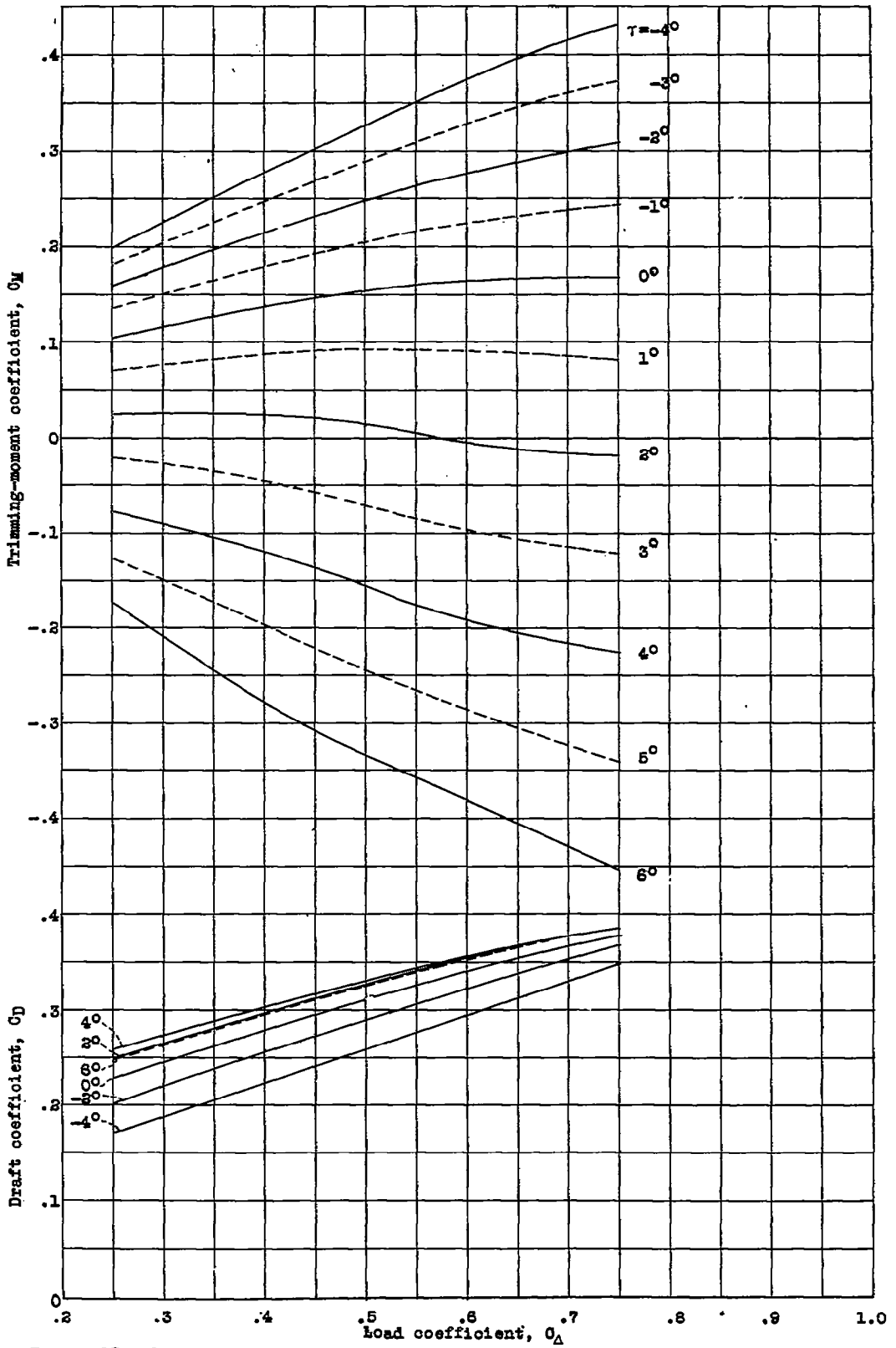

Figure 17.- Trimming-moment coefficient and draft coefficient at rest. Model 82-AD.

Arrows show approximate direction of spray at its origin.

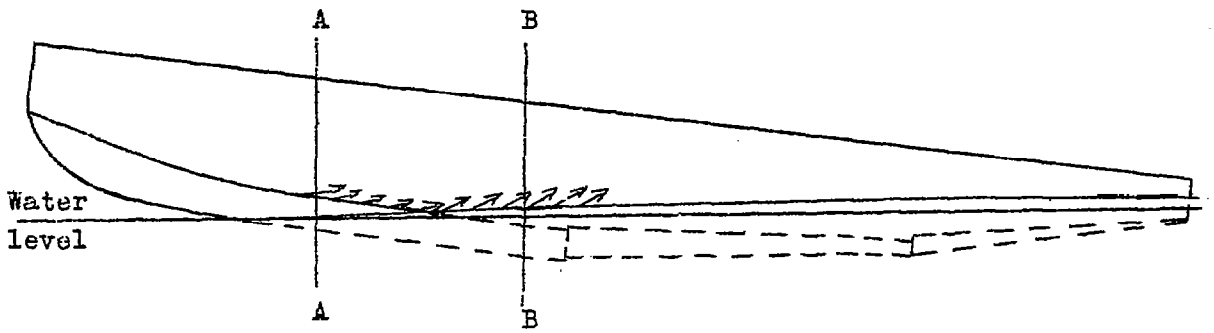

Profile

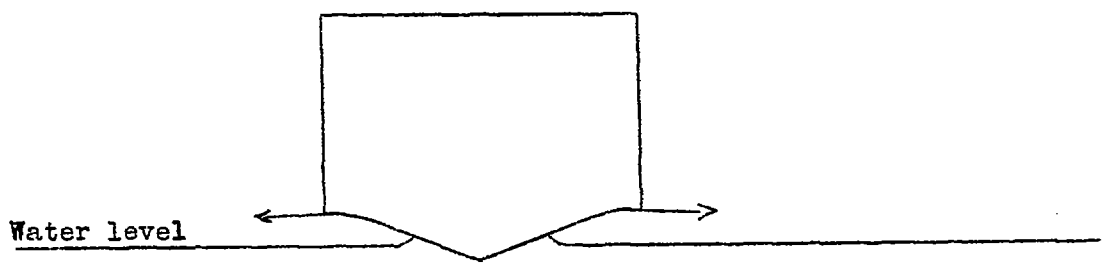

Section A-A

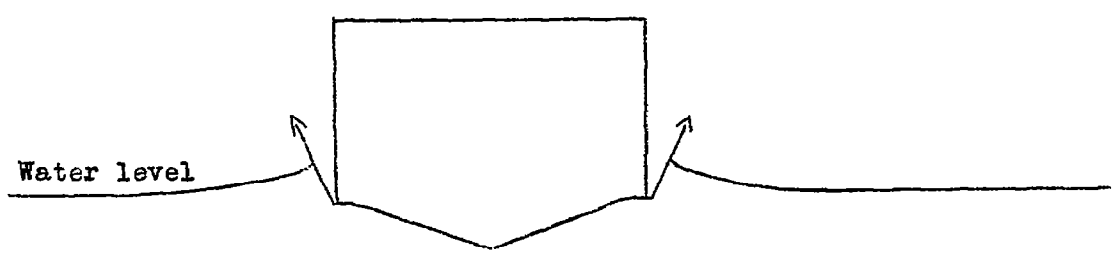

Section B-B

Figure 18.- Diagrams of spray formation at two parts of a typical forebody.

Model 62-D
No flare

Model 62-AD
$f=0.083b_1$
$a=5^\circ$

Model 69-AD
$f=0.083b_1$
$a=15^\circ$

Model 69-BD
$f=0.083b_1$
$a=30^\circ$

Figure 19.- Spray photographs; $\tau = 11^\circ$, $C_V = 2.37$, $C_\Delta = 0.51$.

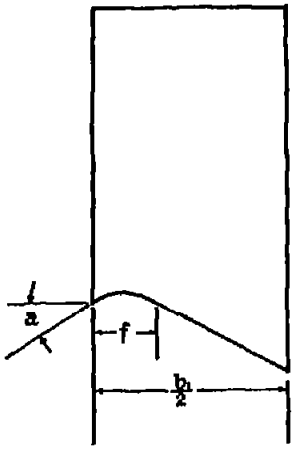

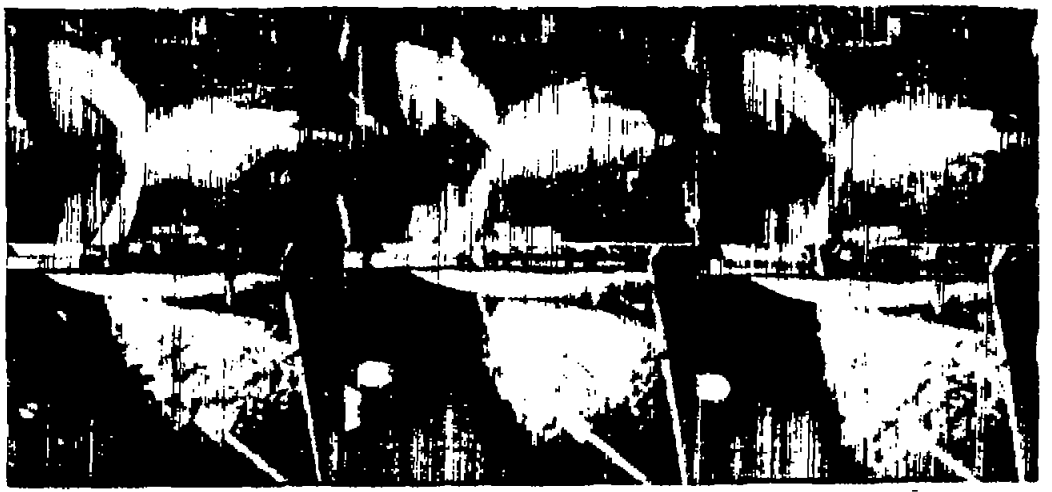

Model 69-CD
$f=0.083b_1$
$a=45^\circ$

Model 69-DD
$f=0.125b_1$
$a=15^\circ$

Model 69-ED
$f=0.125b_1$
$a=30^\circ$

Model 62-D
No flare

Model 62-AD
$f=0.083b_1$
$a=5^0$

Model 69-AD
$f=0.083b_1$
$a=15^0$

Model 69-BD
$f=0.083b_1$
$a=30^0$

Figure 20.- Spray photographs; $\tau=5^0$, $C_T=2.96$, $C_\Delta=0.45$.

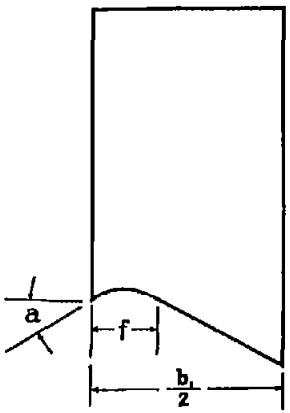

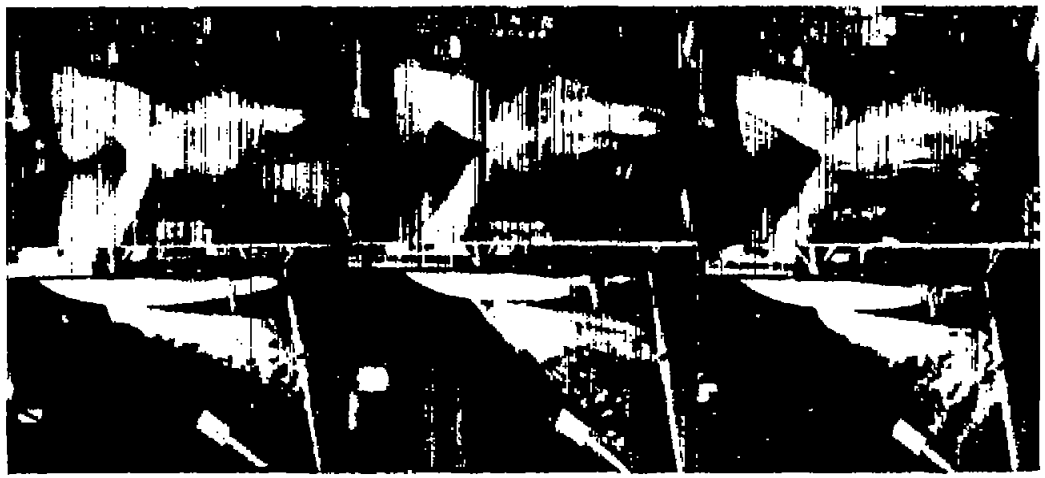

Model 69-CD
$f=0.083b_1$
$a=45^0$

Model 69-DD
$f=0.125b_1$
$a=15^0$

Model 69-ED
$f=0.125b_1$
$a=30^0$

Figure 21.- Spray photographs; $\tau=5^{\circ}$, C_V 5.19, $C_\Delta=0.17$.

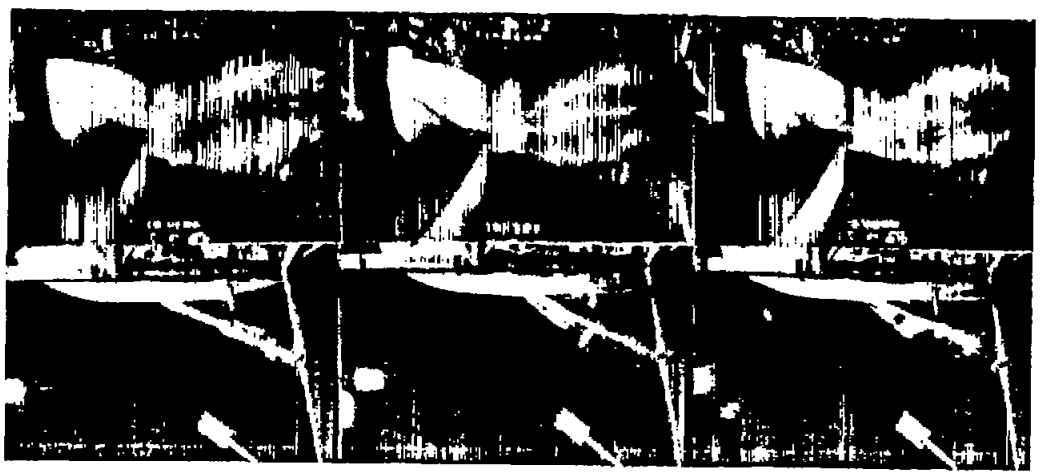

Model 62-D
No flare

Model 62-AD
$f=0.083b_1$
$a=5^{\circ}$

Model 69-AD
$f=0.083b_1$
$a=15^{\circ}$

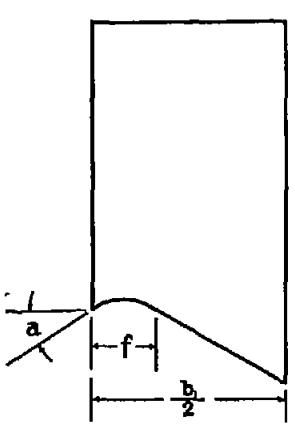

Model 69-CD
$f=0.083b_1$
$a=45^{\circ}$

Model 69-DD
$f=0.125b_1$
$a=15^{\circ}$

Model 69-ED
$f=0.125b_1$
$a=30^{\circ}$